AIAA JOURNAL
Vol. 34, No. 12, December 1996

Boundary-Layer Stability Measurements in a Hypersonic Quiet Tunnel

Jason T. Lachowicz* and Ndaona Chokani†
North Carolina State University, Raleigh, North Carolina 27695-7910
and
Stephen P. Wilkinson‡
NASA Langley Research Center, Hampton, Virginia 23681

Hypersonic boundary-layer measurements were conducted over a flared cone in a quiet wind tunnel. The flared cone was tested at a freestream unit Reynolds number of 2.82×10^6/ft in a Mach 6 flow. This Reynolds number provided laminar-to-transitional flow over the model in a low-disturbance environment. Point measurements with a single hot wire using a novel constant voltage anemometry system were used to measure the boundary-layer disturbances. Surface temperature and schlieren measurements were also conducted to characterize the laminar-to-transitional state of the boundary layer and to identify instability modes. Results suggest that the second mode is the dominant mode of instability. The integrated growth rates of the second mode compared well with linear stability theory in the linear stability regime. Furthermore, the existence of higher harmonics of the fundamental suggests that nonlinear disturbances are not associated with "high" freestream disturbance levels.

Nomenclature

A = disturbance rms amplitude (square root of the power spectral density, arbitrary units)
f = frequency, kHz
R = $(Re_s)^{1/2}$
Re_s = Reynolds number based on freestream conditions and surface distance from the apex of the cone S
r_b = base radius of cone
S = distance along the surface of the model, measured from the apex of the cone model
T_o = total temperature
T_w = surface static temperature
V_s = constant voltage anemometer output voltage
X = coordinate along the cone model axis of symmetry, measured from the apex of the cone
Y = coordinate perpendicular to the cone axis of symmetry, measured from the cone axis of symmetry
Y_w = Y location of the wall surface
$-\alpha_i$ = nondimensional amplification rate, $-\alpha_i = (1/2A)(dA/dR)$
δ = boundary-layer thickness
η = nondimensional Y distance, $\eta = [(Y - Y_w)R/S]$
λ = disturbance wavelength
ρU = mass flux

Subscripts

o = neutral stability first branch location
u = most upstream measurement location
∞ = conditions in freestream

Superscripts

$'$ = fluctuating component of a time-dependent quantity
$\overline{()}$ = time average of a particular quantity

Received Dec. 21, 1995; revision received July 26, 1996; accepted for publication July 26, 1996; also published in *AIAA Journal on Disc*, Volume 2, Number 1.

*Graduate Research Assistant, Department of Mechanical and Aerospace Engineering; currently National Research Council Associate, NASA Langley Research Center, Hampton, VA 23681. Member AIAA.
†Associate Professor, Department of Mechanical and Aerospace Engineering. Member AIAA.
‡Research Engineer, Flow Modeling and Control Branch. Senior Member AIAA.

Introduction

THE change from laminar to turbulent flow in the hypersonic boundary layer is accompanied by large changes in both heat transfer and skin-friction drag. These changes are important to the aerodynamic design of hypersonic vehicles because the aerodynamic coefficients are very sensitive to the large changes in heat transfer and skin friction that accompany transition.[1] Furthermore, the stability, control, and structural design of the vehicle are affected due to the increased thermal and aerodynamic loading.

The conical geometry is prevalent in many hypersonic aerodynamic applications, but only a few stability experiments[2] of hypersonic cone boundary layers have been conducted. These studies have provided a fundamental understanding of the hypersonic boundary-layer stability problem. However, these few stability experiments have been conducted in conventional hypersonic wind tunnels where relatively large freestream disturbances occur. The primary source of the freestream disturbances is acoustic radiation from convecting eddies generated by the turbulent boundary layer on the nozzle wall.[3,4] The frequency content of this incident noise field provides a stimulus to excite disturbances in the hypersonic boundary layer, which may lead to transition. Thus, some of the observed anomalies between experiment and theory[5,6] may be due to effects of the wind-tunnel noise.

To provide a more reliable test environment for the experimentalist, the NASA Langley Research Center has developed a series of supersonic/hypersonic quiet tunnels.[7] In these facilities, the freestream noise is maintained at low levels by treating the settling chamber flow and maintaining the nozzle wall boundary layer in a laminar state. Hence, transition on the nozzle wall is delayed, providing lower freestream disturbance levels in the quiet tunnel relative to conventional tunnels.

This is the first paper to document hypersonic boundary-layer stability measurements obtained in a quiet tunnel. The primary objective of this work is to provide experimental stability data in a low-disturbance environment. Such data may be better suited for comparison with stability theory data.

Experimental Apparatus

Test Facility

All tests were conducted in the NASA Langley Nozzle Test Chamber Facility. This is an open-jet blowdown facility and was equipped for the present tests with a slow-expansion, axisymmetric, quiet Mach 6 nozzle. The nozzle, which is more fully described in Ref. 8, had a throat diameter of 1.00 in. (2.54 cm), exit diameter of 7.49 in.

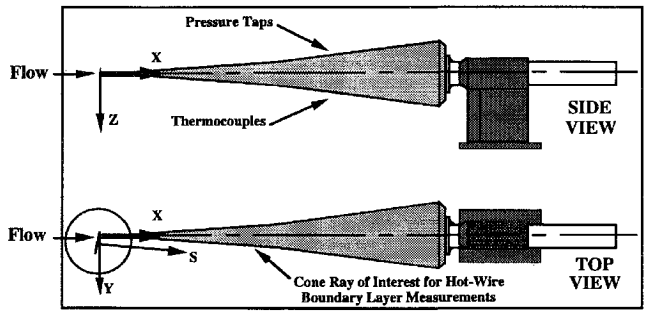

Fig. 1 Flared cone.

(19.02 cm), and length from throat to exit of 39.76 in. (100.99 cm). The nozzle is equipped with an annular throat slot to remove the boundary layer that develops upstream of the throat, a straight nozzle contour section, and a highly polished nozzle surface. As a result, the boundary layer that forms on the nozzle wall remains in a laminar state until far downstream. This provides low disturbance levels in the nozzle test section. The nozzle may be operated over a range of stagnation pressures from 80 to 200 psia (551 to 1379 kPa) and stagnation temperatures up to 400°F (204°C). Run times from minutes to several hours are possible. The freestream disturbance environment of the quiet tunnel used in the present work is documented in Ref. 9.

Test Model

The model, used in this study, was a 20-in. (50.80-cm)-long cone with a curved-flare afterbody shown in Fig. 1. For sake of brevity, this model is referred to as the flared cone. The straight cone surface extended from $X = 0$ to $X = 10$ in. (25.40 cm), with a semivertex angle of 5 deg. The flare surface radius of curvature was 93.07 in. (236.40 cm) and extended from $X = 10$ in. (25.40 cm) to 20 in. (50.80 cm). The base diameter was 4.6 in. (11.68 cm). The sharp model tip had a nominal radius of 0.0001 in. The model surface was instrumented with 29 pressure orifices and 51 thermocouple gauges.

The flared cone was used instead of a straight cone to induce transition on the model within the quiet flow region of the tunnel. The flare generated an adverse pressure gradient resulting in a reduced boundary-layer thickness compared with a straight cone at the same freestream conditions. Thus, in comparison to the straight cone, the effects of the flare are expected to be as follows[10]: 1) the amplification rates for both first- and second-mode disturbances are increased; 2) the frequencies of the most amplified second mode increased; 3) the frequencies of the most amplified first-mode disturbances do not change significantly; and 4) curvature effects are negligible. These effects should be considered when attempting to use the results presented in this study to explain the previously observed discrepancies between straight cone experimental[5] and theoretical data.[6]

The maximum rms deviation of the model was 0.1% of the model base radius, or about 2.8% of the model boundary-layer thickness near the model base. Thus, the model surface was quite smooth and any possible effects of roughness-induced transition are minimal.

Hot-Wire Probes

The hot-wire probes were constructed of platinum-rhodium (10%) wire of 100-μin. (25.4-μm) diam. The wire was soldered onto 0.005-in. (0.127-mm)-diam stainless steel broaches that were attached to the main probe body. The nominal length-to-diameter ratio of the wire was 150. The wire was slack to minimize the strain-gauge effect. An electrical contact probe was located about 0.005 in. (0.127 mm) below the broaches to determine the location of the model surface.

Hot-Wire Anemometer

The hot-wire anemometer system used in the present work was a novel constant voltage anemometer (CVA). In this system, a steady dc voltage was maintained across the hot wire through the use of a composite-amplifier-compensation circuit. The operating principles of the CVA are described in detail in Ref. 11. The static responses of the CVA for subsonic and supersonic flows are discussed in Refs. 12 and 13, respectively. Only the CVA, in contrast to attempts with constant current and constant temperature anemometers, provided the ability to obtain measurable signals in the freestream of the quiet nozzle flow since the CVA was less susceptible to electromagnetic noise. The present CVA system had a bandwidth of about 400 kHz with a 40 dB/decade rolloff.

The CVA operation was computer controlled for all tests conducted. For the mean and rms measurements, the wire voltage was automatically changed through seven levels at each boundary-layer measurement location; the voltage magnitudes were optimized for the individual wires used. The constant wire voltage was monitored throughout testing using a $5\frac{1}{2}$ digit digital multimeter. The multimeter was also used to measure the mean CVA output signal. The rms and fluctuating components were measured from the ac-coupled CVA output signal. An analog true rms voltmeter was used to determine the CVA rms output voltage. Prior to measurement, the CVA output was high-pass filtered at 1 kHz and low-pass filtered at 1 MHz. A 12-Bit digital oscilloscope was used to obtain time traces of the fluctuating CVA output voltage at constant overheat.[14] The high- and low-pass filter settings were 100 Hz and 1 MHz, respectively, and the sampling rate was 2 MHz; 2^{17} points were sampled at each location. Standard fast Fourier transform procedures employing a Hanning window, data length of 512 points, and 256 (i.e., $2^{17}/512$) averages were used to obtain the spectra.

A calibration procedure for the CVA was developed and is outlined in Ref. 15. This procedure enabled mean and rms mass flux and total temperatures in the boundary layer to be obtained. The comparisons of the present data with computational predictions verified the validity of the procedure for mean flow quantities. However, the accuracy of the quantitative rms data could not be verified for the fixed-time-compensation CVA system. Nevertheless, the absence of quantitative fluctuation data did not prevent an analysis of the spatial amplification rates in the linear and weakly nonlinear stability regimes. In the linear stability region, fluctuations are expected to grow (or decay) exponentially. This exponential growth is described by normal mode decomposition,[5] which specifies that the amplification rate is the same for separate fluctuation components (pressure, velocity, etc.). Thus, an uncalibrated approach is valid in the linear stability region as verified from both controlled[16] and uncontrolled[6] stability experiments. In the weakly nonlinear stability regime, analysis of the present data indicated that the experimentally derived amplification rates are mainly of a mass-flux nature.[15]

Experimental Approach

Test Conditions

The stagnation conditions for the present tests were a temperature of 810°R and a pressure of 130.0 ± 0.2 psia (896.3 ± 1.38 kPa). The measured freestream Mach number was 5.91. These conditions yielded a freestream unit Reynolds number of $(2.82 \pm 0.02) \times 10^6$/ft [$(0.859 \pm 0.006) \times 10^6$/m].

Prior to the present tests, the characteristics of the freestream flow were documented through a series of pitot-probe and hot-wire measurements. The details of the freestream measurements are presented in Refs. 9 and 15, but a few salient features are presented here. The pitot-probe surveys verified that the nozzle mean flow was uniform within the flow hot-wire test volume. Within this volume the Mach number was 5.91 ± 0.08. Measurements in cross-sectional planes indicated that the mean flow was axisymmetric and varied by no more than 1% in the test volume, which encompassed the model. The data showed that the low-level disturbance field was axisymmetric and was associated with sound-mode generation of the nozzle wall turbulent boundary layer.

Measurements

The measurements were conducted in two stages. First, model surface temperature and schlieren imaging measurements were conducted, and then hot-wire boundary-layer surveys were conducted. The surface temperature measurements were used to verify that the model was in thermal equilibrium and to estimate the location of transition onset. The schlieren images were used to verify the

laminar-to-transitional state of the boundary layer and to identify the character of the instability modes.

Preliminary hot-wire boundary-layer surveys were conducted at 17 streamwise stations, spaced 0.5 in. (1.27 cm) apart over the range $X = 10.97$ ($R = 1610$) to 18.97 in. (2120). At each streamwise station, the wire was traversed perpendicular to the cone axis of symmetry. The mean and rms measurements were obtained at 13 points clustered near the boundary-layer edge. At each measurement point, seven wire voltages were applied. The rms profiles were then inspected to determine the maximum energy (rms) location at the given streamwise station. Wave traces were subsequently measured at the maximum energy locations using the maximum, practicable wire voltage. At this operating condition, the CVA is more sensitive to changes in the mass flux than to changes in the total temperature.[13,15] In addition, the CVA signal-to-noise ratio is improved.

From the preliminary data, it was determined that the second mode was first measurable at about $X = 15$ in. ($R \cong 1880$). Thus, subsequent measurements were conducted at a greater resolution, 0.25-in. (0.625-cm) streamwise increments, from $X = 14.96$ ($R \cong 1880$) to 18.96 in. ($R \cong 2120$). The same procedure outlined in the previous paragraph was followed for these measurements; all fluctuation data presented in this paper are for these latter measurements.

The N factor, or integrated growth rate, was computed from the following equation:

$$N = \ln A\Big|_{X_o}^{X} = \ln A\Big|_{X_u}^{X} + \ln A\Big|_{X_o}^{X_u}$$

where the second term on the right-hand side is the integrated growth rate from X_o to X_u as determined from LST (linear stability theory).[10] The spatial amplification rates were computed as follows. For each frequency, the amplitude A was curvefit with respect to R. Since the functional dependence of A with respect to R differed greatly for individual frequencies, a fairly general curvefit was chosen for the purpose of fitting the A vs R data. The curvefit was a cubic smoothing spline that contained a parameter to control the amount of data smoothing. The smoothing parameter was chosen so that the cubic smoothing spline interpolant contained as much of the essential characteristics of the amplitude profile as possible but as little of the supposed noise. Using the spline fit coefficients for the fitted function, the derivative, dA/dR, was then computed for each frequency. Then, the nondimensional amplification rate was computed for each frequency according to the following equation:

$$-\alpha_i = \frac{1}{2A}\frac{dA}{dR}$$

Results

Noisy vs Quiet Tunnel Comparison

To better understand the quiet and noisy tunnel operation modes, a few salient features of the noisy mode of operation are discussed next.

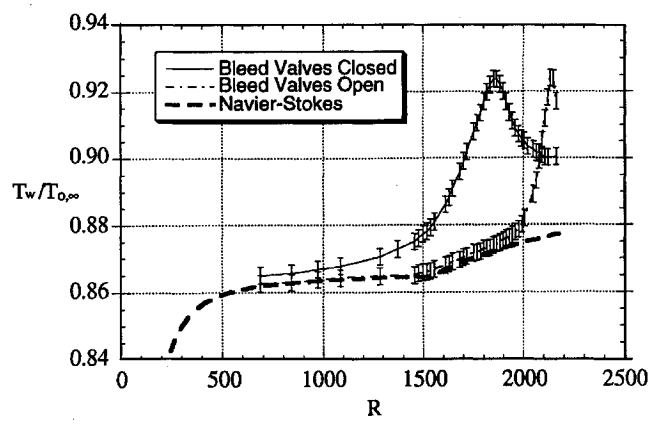

Fig. 2 Comparison of surface temperature data for bleed valves open and closed.

The surface temperature data with the tunnel operated in the bleed valves closed (noisy) and bleed valves open (quiet) modes are compared with Navier–Stokes predictions[15] in Fig. 2. For the upstream locations, $R < 1000$, both the bleed valves open (BVO) data and bleed valves closed data (BVC) compare well with the theoretical data, as expected. The sharp rise in experimental temperature relative to the theoretical (laminar) temperature indicates a transitional boundary layer because a transitioning boundary layer is heated and some of this heat is convected to the wall via turbulent vortices that heat the model surface. Comparing the sharp temperature rise regions for each mode, the BVC transition onset location ($R \cong 1575$) is upstream of the BVO transition onset location ($R \cong 1975$); an estimate of transition onset was determined by the intersection point of two straight lines passing through the laminar region and sharp temperature rise region. Along the nozzle wall, the boundary layer is fully turbulent for the BVC mode, producing substantially higher levels of acoustic disturbances relative to the BVO mode where the nozzle wall boundary layer is laminar-to-transitional. This causes transition to move upstream along the model for the BVC mode relative to the BVO mode as shown in Fig. 2. Thus, similar upstream movement would occur in a conventional tunnel at the same test Reynolds number and Mach number. (To circumvent this problem, stability experiments in conventional tunnels are conducted at lower Reynolds numbers where the nozzle wall acoustic radiation is minimal.)

The fluctuation spectra for the BVC mode of operation is presented in Fig. 3 at the maximum energy locations. From $R = 1610$ to 2005, the boundary layer is clearly transitional with disturbance energy distributed over a fairly wide frequency range from 0 to 400 kHz and peak energy (i.e., maximum amplitudes) in the 0–20 kHz range. Observing Fig. 2, this R range corresponds to both the sharp temperature rise region associated with transition onset and the subsequent temperature decrease associated with the initial stages of fully turbulent flow. For $R > 2005$, the disturbance energy continues to spread to higher frequencies, suggesting a fully turbulent boundary layer. This turbulent region compares well with the surface temperature data of Fig. 2; the temperature is relatively constant for $R > 2005$, reflecting a fully turbulent boundary layer.

The rest of the results presented in this study are for the BVO case (quiet mode of operation). Schlieren measurements (not presented here) verified the laminar-to-transitional boundary-layer state seen from the surface temperature data. A wavy structure near the edge of the boundary layer was identified in the schlieren data. The wavelength of this structure was measured to be approximately twice the boundary-layer thickness, identifying the structure as a second mode disturbance.[6]

Boundary-Layer Mean Data

The experimental and computational boundary-layer thickness distributions are presented in Fig. 4. Note that the computational[15] boundary-layer thickness distribution was curvefit using a second-order polynomial, and the experimental error is ±2% of the plotted values. Upstream, $R = 1610-1915$, the experimental and computational boundary-layer thicknesses compare well as expected. From $R = 2000$ to 2120, the experimental δ becomes greater than the computational δ, confirming the transitional nature of the boundary

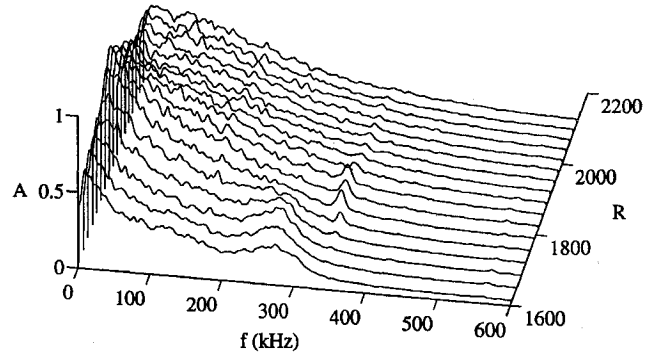

Fig. 3 Fluctuation spectra at locations of maximum energy: bleed valves closed.

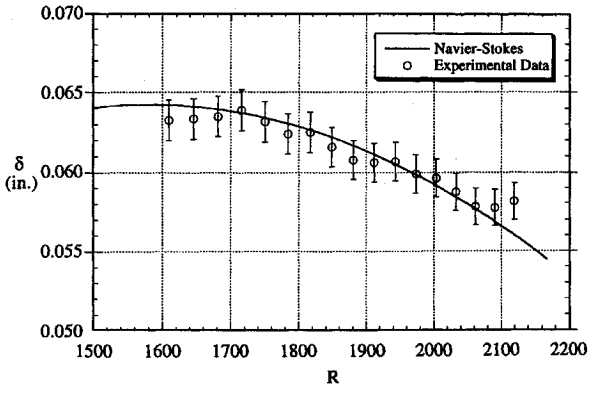

Fig. 4 Boundary-layer thickness distribution.

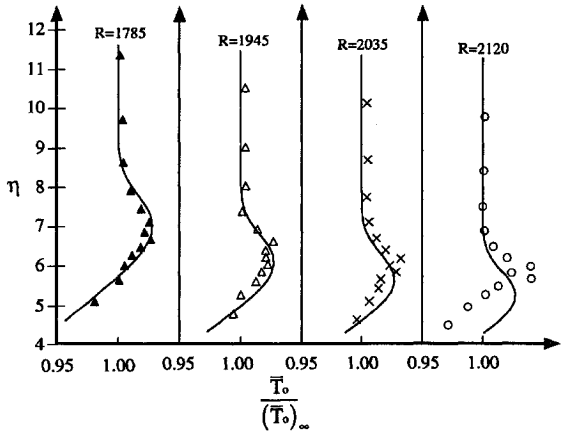

Fig. 5 Total temperature profiles.

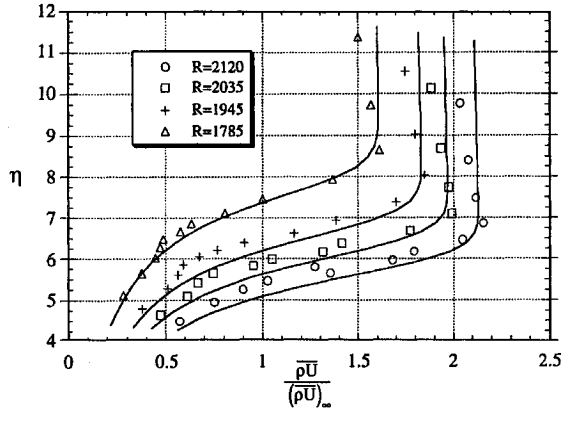

Fig. 6 Mass-flux profiles.

layer over this region. This transitional region is seen more clearly with the aid of Figs. 5 and 6, which are discussed next.

The experimental mean total temperature and mass flux profiles are presented in Figs. 5 and 6 at four streamwise locations. Also, laminar total temperature and mass flux profiles, computed from the Navier–Stokes code of Ref. 17, are presented as the solid lines in Figs. 5 and 6. At $R = 1785$ and 1945, the experimental and computational data compare well. The good agreement with computational data at these locations is typical of all total temperature and mass flux data over the range $1610 \leq R \leq 1945$ and is consistent with the boundary-layer thickness data. From $1945 \leq R \leq 2035$, the departure from laminar flow is difficult to discern from the mean data. However, at $R = 2035$, the total temperature and mass flux show evidence of mean flow distortion from about $\eta = 5.09\,(0.734\,\delta)$ to 6.39 $(0.921\,\delta)$. At the most downstream location, $R = 2120$, the lower portion of the boundary-layer region is distorted from $\eta = 4.49\,(0.680\,\delta)$ to 6.18 $(0.935\,\delta)$, marking a high fluctuating

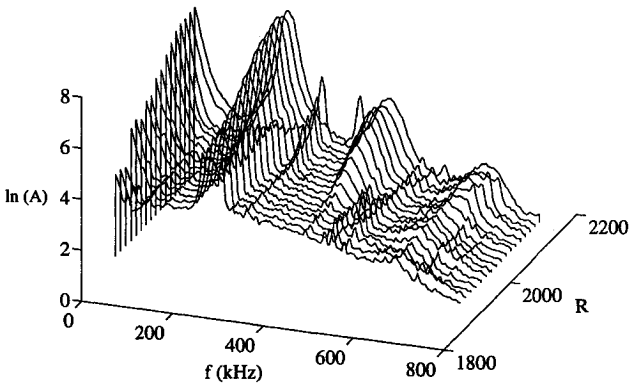

Fig. 7 Fluctuating spectra at maximum energy locations.

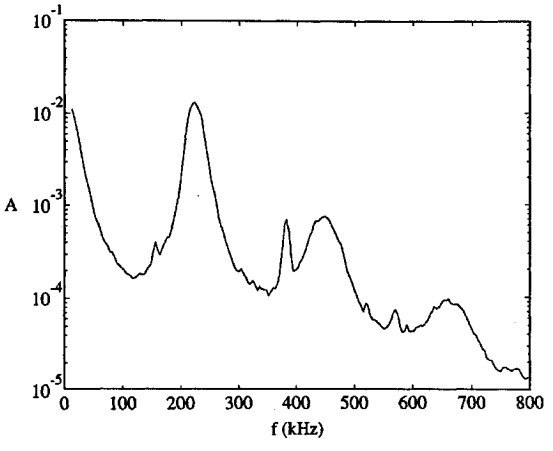

Fig. 8 Fluctuation spectra at R = 2120.

disturbance region. Overall, the mean flow is distorted in the range, (0.71–0.93) δ, which is in the vicinity of the critical layer.

Boundary-Layer Fluctuation Data

The fluctuation spectra are presented in Fig. 7 at the maximum energy locations. The second-mode is clearly discernible in the range 180–260 kHz. The growth of the second mode disturbances surpasses the growth of any other disturbance, indicating the dominance of the second mode. Over the upstream linear stability region, $1875 \leq R \leq 2050$, the second-mode growth is exponential as expected. Growth of the second-mode harmonics[18] can also be seen.

For clarity, these second-mode harmonics are presented in Fig. 8, which presents the fluctuation spectra at the most downstream location surveyed, $R = 2120$. At this streamwise location, the maximum amplitudes for the second mode, first harmonic, and second harmonic occur at 226, 449, and 670 kHz, respectively. Emerging theoretical approaches[19,20] do not show any direct evidence of dominant harmonics. However, previous measurements in conventional tunnels,[18] as well as the present test, show second-mode higher harmonic growth. Thus, the higher harmonics are not associated with high freestream disturbance levels.

The N factor, or integrated growth rates, are presented at select frequencies in Fig. 9. (The LST integrated growth rate, $\ell_n A|_{X_o}^{X_u} = 6.015$, at the most upstream measurement location was added to the experimental integrated growth rates.) The positive, constant slope line regions mark the linear stability regime, or exponential growth region. For the frequencies 215–230 kHz, the linear stability regime spans the range $1880 \leq R \leq 2060$. For $f = 220$ kHz, the change in LST[10] N factor is 3.10 for the range $1880 \leq R \leq 2060$, comparing within 1.5% of the experimental N factor of 3.05. The slope for this frequency also compares well with LST, which is presented as the solid line. For $f = 230$ kHz, the change in LST integrated growth rate is 3.09 for the range $1880 \leq R \leq 2060$, comparing within 5% of the experimental N factor of 2.94. (Defining the weakly nonlinear region as the region from the downstream end of the linear regime

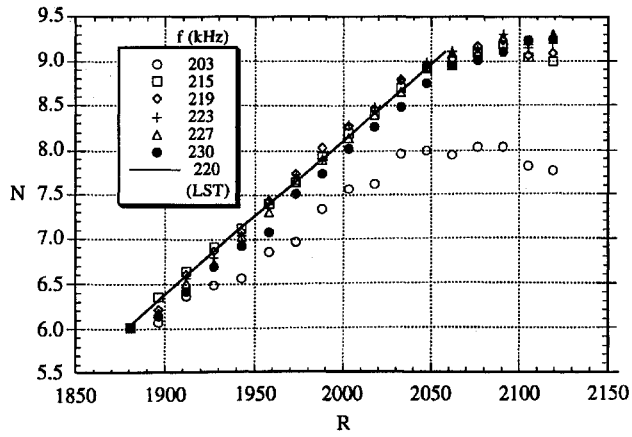

Fig. 9 Second-mode N factors at select frequencies.

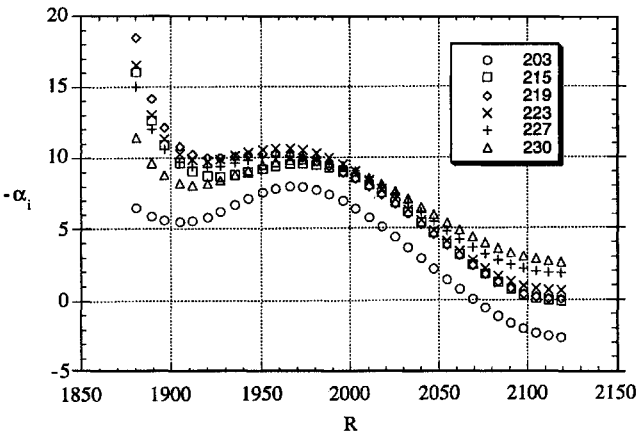

Fig. 10 Second-mode amplification rates at select frequencies.

to the location where the slope of N is zero, it can be seen that this region extends from $R = 2060$ to 2120.) In summary, these results suggest that excellent comparison in terms of integrated growth rates is obtained in a quiet wind tunnel in the linear stability regime.

The amplification rates for the N factor presented in Fig. 9 are presented in Fig. 10. Over the range $1900 \leq R \leq 1980$, the amplification rates are approximately constant for $f = 215$–230 kHz. This is expected since the region were the N factor is constant in Fig. 9 denotes constant $-\alpha_i$ regions. Farther downstream, $R > 2050$, the decrease in amplification rate is expected from the data in Fig. 9. Over this region, the flow is becoming nonlinear as observed by the higher harmonics in Fig. 7 and the mean flow distortion of Figs. 5 and 6.

Concluding Remarks

The first hypersonic boundary-layer stability measurements in a quiet wind tunnel have been obtained. All test cases were conducted at a freestream Mach number of 5.91 and freestream unit Reynolds number of 2.82×10^6/ft in the NASA Langley Research Center's Nozzle Test Chamber Facility. The second-mode disturbances dominate the transition process. The second-mode integrated growth rates compare within 5% of linear stability theory in the linear stability regime. Furthermore, the existence of higher harmonics of the fundamental suggests that nonlinear disturbances are not associated with high freestream disturbance levels.

Acknowledgments

This work was supported by Cooperative Agreement NCC1-183 between North Carolina State University and NASA Langley Research Center. The constant voltage anemometer (CVA) system used in this work was developed by Tao Systems. The authors are grateful to G. R. Sarma, of Tao Systems, for providing assistance with the CVA. The authors gratefully acknowledge the close collaboration of A. E. Blanchard.

References

[1]Finley, D., "Hypersonic Aerodynamic Considerations and Challenges," AIAA Paper 90-5222, Oct. 1990.

[2]Stetson, K. F., and Kimmel, R. L., "On Hypersonic Boundary-Layer Stability," AIAA Paper 92-0737, Jan. 1992.

[3]Laufer, J., "Aerodynamic Noise in Supersonic Wind Tunnels," *Journal of the Aerospace Sciences*, Vol. 28, No. 9, 1961, pp. 685–692.

[4]Morkovin, M. V., "On Supersonic Wind Tunnels with Low Free-Stream Disturbances," *Journal of Applied Mechanics*, Vol. 26, Sept. 1959, pp. 319–324.

[5]Mack, L. M., "Stability of Axisymmetric Boundary Layers on Sharp Cones at Hypersonic Mach Numbers," AIAA Paper 87-1413, June 1987.

[6]Stetson, K. F., Thompson, E. R., Donaldson, J. C., and Siler, L. G., "Laminar Boundary Layer Stability Experiments on a Cone at Mach 8, Part 1: Sharp Cone," AIAA Paper 83-1761, July 1983.

[7]Wilkinson, S. P., Anders, S. G., Chen, F.-J., and White, J. A., "Status of NASA Langley Quiet Flow Facility Developments," AIAA Paper 94-2498, June 1994.

[8]Chen, F.-J., Wilkinson, S. P., and Beckwidth, I. E., "Görtler Instability and Hypersonic Quiet Nozzle Design," *Journal of Spacecraft and Rockets*, Vol. 30, No. 2, 1993, pp. 170–175.

[9]Blanchard, A. E., Lachowicz, J. T., and Wilkinson, S. P., "Performance of the NASA-Langley Mach 6 Quiet Wind Tunnel," AIAA Paper 96-0441, Jan. 1996.

[10]Balakumar, P., and Malik, M. R., "Effects of Adverse Pressure Gradient and Wall Cooling on Instability of Hypersonic Boundary Layers," High Technology Corp., Rept. 9404, Hampton, VA, March 1994.

[11]Sarma, G. R., "Analysis of a Constant Voltage Anemometer Circuit," *Proceedings of the IEEE Instrumentation and Measurement Technology Conference* (Irvine, CA), IEEE No. 93CH329, Inst. of Electrical and Electronics Engineers, Piscataway, NJ, 1993, pp. 730–736.

[12]Comte-Bellot, G., "Hot-Wire Anemometry," *Handbook of Fluid Dynamics*, Oxford Univ. Press, New York (to be published).

[13]Kegerise, M. A., and Spina, E. F., "A Comparative Study of Constant-Voltage and Constant-Temperature Hot-Wire Anemometers in Supersonic Flow," *Proceedings of the Fluid Engineering Division Conference*, FED-Vol. 239, Vol. 4, American Society of Mechanical Engineers, New York, 1996, pp. 297–308.

[14]Blanchard, A. E., "An Experimental Investigation of Wall Cooling Effects on Hypersonic Boundary-Layer Stability in a Quiet Wind Tunnel," Ph.D. Dissertation, Dept. of Mechanical Engineering, Old Dominion Univ., Norfolk, VA, Dec. 1995.

[15]Lachowicz, J. T., "Hypersonic Boundary Layer Stability Experiments in a Quiet Wind Tunnel with Bluntness Effects," Ph.D. Dissertation, Mechanical and Aerospace Engineering Dept., North Carolina State Univ., Raleigh, NC, Nov. 1995.

[16]Kendall, J. M., "Some Comparisons of Linear Stability Theory with Experiment at Supersonic and Hypersonic Speed," *Instability and Transition*, edited by M. Y. Hussaini and R. G. Voigt, Vol. 1, Springer–Verlag, New York, 1989, pp. 68–76.

[17]Edwards, J. R., "A Low-Diffusion Flux-Splitting Scheme for Navier–Stokes Calculations," AIAA Paper 95-1703, June 1995.

[18]Kimmel, R. L., and Kendall, J. M., "Nonlinear Disturbances in a Hypersonic Laminar Boundary Layer," AIAA Paper 91-0320, Jan. 1991.

[19]Chang, C.-L., and Malik, M. R., "Non-Parallel Stability of Compressible Boundary Layers," AIAA Paper 93-2912, July 1993.

[20]Pruett, C. D., "Direct Numerical Simulation of Laminar Breakdown in High-Speed, Axisymmetric Boundary Layers," AIAA Paper 92-0742, Jan. 1992.